Wavelet Analysis and Filtering to Identify

Dominant Orientations of Permeability Anisotropy [1]

Loring Watkins [2] Roseanna M. Neupauer [*,3] and Gilbert P. Compo [4]

Abstract

An accurate representation of permeability anisotropy is needed to correctly model the rate and direction of groundwater flow. We develop a wavelet analysis technique that can be used to characterize principal directions of anisotropy in both stationary and non-stationary permeability fields. Wavelet analysis involves the integral transform of a field using a wavelet as a kernel. The wavelet is shifted, scaled, and rotated to analyze different locations, sizes, and orientations of the field. The wavelet variance is used to identify scales and orientations that are dominant anywhere in the field. If the field is non-stationary, such that different zones of the field are characterized by different dominant scales or orientations, the wavelet variance can identify all dominant scales and orientations if they are distinct. If the dominant scales and orientations of different zones are similar, the wavelet variance only identifies the dominant scale and orientation of the primary zone. In this paper, we present a combined wavelet analysis and filtering approach to identify all dominant scales and orientations in a non-stationary permeability field. We apply the method to laboratory-collected permeability data from Massillon sandstone.

Key words: heterogeneity, non-stationary, Morlet wavelet

INTRODUCTION

Porous medium properties, such as permeability, are often spatially variable and anisotropic. In a layered porous medium, permeability varies with direction, with the highest and lowest permeabilities found in the directions parallel and perpendicular to layering, respectively. These directions are called the principal directions of anisotropy.

Fluid flow in porous media is described by Darcy's law, given by

$$\begin{bmatrix} q_x \\ q_y \end{bmatrix} = -\frac{\rho g}{\mu} \begin{bmatrix} k_{xx} & k_{xy} \\ k_{yx} & k_{yy} \end{bmatrix} \begin{bmatrix} \partial h/\partial x \\ \partial h/\partial y \end{bmatrix}, \tag{1}$$

where q_x and q_y are components of specific discharge in the x and y directions, respectively, ρ is the fluid density, g is the gravitational constant, μ is the fluid viscosity, k_{ij} is the i,jth entry of the permeability tensor, and $\partial h/\partial x$ and $\partial h/\partial y$ are the hydraulic gradients in the x and y directions, respectively. The components of the permeability tensor are given by (Bear, 1972)

$$k_{xx} = \frac{k_\parallel + k_\perp}{2} + \frac{k_\parallel - k_\perp}{2}\cos(2\theta) \tag{2}$$

$$k_{yy} = \frac{k_\parallel + k_\perp}{2} - \frac{k_\parallel - k_\perp}{2}\cos(2\theta) \tag{3}$$

$$k_{xy} = k_{yx} = \frac{k_\parallel - k_\perp}{2}\sin(2\theta) \tag{4}$$

* Email address: neupauer@colorado.edu

[1] Received ; accepted .

[2] University of Colorado at Boulder; Now at Lytle Water Solutions, LLC, Highlands Ranch, Colorado

[3] University of Colorado at Boulder

[4] University of Colorado at Boulder, CIRES/Climate Diagnostics Center, and NOAA Earth System Laboratory/Physical Sciences Division

where $k_{\parallel}$ is the average permeability parallel to layering, $k_{\perp}$ is the average permeability perpendicular to layering, and θ is the orientation of layering, which we call the dominant orientation. If the assumed value of the dominant orientation of the permeability tensor is incorrect, the magnitude and direction of the specific discharge from (1) will also be incorrect, with errors in magnitude of up to 30% and errors in flow direction of up to 45° (Anderman et al., 2002). The errors increase as the anisotropy ratio, $k_{\parallel}/k_{\perp}$, increases.

Several studies demonstrate the importance of an accurate representation of aquifer anisotropy. Anisotropy was shown to have significant effects on the patterns of groundwater seepage from lakes (Genereux and Bandopadhyay, 2000), on groundwater travel times in sedimentary fractured rocks (Burton et al., 2002), on seepage in bog peat (Beckwith, Baird, and Heathwaite, 2003), and on the migration processes of infiltrated stream water to a partially penetrating well (Chen and Chen, 2003).

In this paper, we present a method for identifying dominant orientations in a non-stationary permeability field that exhibits anisotropy. We consider the class of non-stationarity in which the permeability field contains zones with different dominant orientations and scales, but within a given zone, the properties are stationary. We assume that point measurements of permeability are isotropic, but that adjacent permeability measurements are correlated with different correlation lengths in different directions. Thus, the permeability field exhibits structural anisotropy.

Two methods that have been used to determine dominant orientations are directional variograms and anisotropic wavelet analysis. A directional variogram identifies spatial correlation by estimating the variability in permeability as a function of the separation distance between measurements and of the relative orientation of the separations. The dominant orientation is the direction that exhibits correlation through the longest separation distance (Isaaks and Srivastava, 1989). Tidwell and Wilson (2000) use variograms to quantify spatial variability in permeability measurements from a block of Massillon sandstone. The sandstone exhibits layering of bounding surfaces with low permeability that separate cross-stratification sets that have higher permeability. A two-dimensional variogram identified the dominant orientations of each rock face.

Neupauer et al. (2006) developed a wavelet analysis approach to identify dominant orientations of an anisotropic permeability field. In anisotropic wavelet analysis, an integral transform is performed on the permeability data using an anisotropic kernel. The largest value of the integral transform occurs when the orientation of the kernel matches the dominant orientations of the permeability field. If the permeability field is non-stationary, with different dominant orientations at different locations, the method of Neupauer et al. (2006) identified all dominant orientations only if the dominant orientations are distinct. If the dominant orientations are not distinct, the method only identified the primary (most dominant) orientation, while secondary orientations could not be identified.

In this paper, we enhance the wavelet analysis method of Neupauer et al. (2006) to develop a method that identifies both primary and secondary orientation in a non-stationary, anisotropic permeability field. This method uses a combination of wavelet analysis and filtering. The method has been developed for two-dimensional, uniformly-spaced permeability data sets. In the next section, we present wavelet analysis theory, and we introduce the filtering procedure. In the subsequent section, we illustrate the new combined wavelet analysis and filtering method using two-dimensional synthetic data sets. Finally, we apply the method to Tidwell and Wilson's (2000) permeability data from Massillon sandstone.

METHODOLOGY

The methodology used to implement wavelet analysis on a two-dimensional field is explained in this section. We present general wavelet analysis theory, followed by our specific procedure for identifying dominant orientations in a non-stationary random field.

Theory

The continuous wavelet transform of a two-dimensional field, $f(\mathbf{x})$, is given by (e.g., Farge, 1992)

$$W^{\theta}(a, \mathbf{b}, \theta; L) = \int f(\mathbf{x}) \psi^{*}_{a,\mathbf{b},\theta;L}(\mathbf{x}) d\mathbf{x}, \tag{5}$$

where $W^{\theta}(a, \mathbf{b}, \theta; L)$ is the wavelet coefficient, $\psi_{a,\mathbf{b},\theta;L}(\mathbf{x})$ is the scaled, shifted, and rotated two-dimensional wavelet, a is the scaling factor, $\mathbf{x} = (x, y)$ is the spatial domain, $\mathbf{b}$ is the shift vector on the spatial domain (x, y), θ is the angle of orientation of the wavelet relative to the $+x$ axis (positive θ is in the counterclockwise direction), L is the anisotropy ratio, defined as the ratio of the scaling factor in the direction perpendicular to θ to the scaling factor in the θ direction, and the superscript asterisk denotes the complex conjugate. The limits of integration are $-\infty$ to $+\infty$ unless otherwise stated. The scaled, shifted, and rotated wavelet is given by (Farge, 1992)

$$\psi_{a,\mathbf{b},\theta;L}(\mathbf{x}) = \sqrt{\det(\mathbf{A})}\psi(\mathbf{AC}(\mathbf{x}-\mathbf{b})), \tag{6}$$

where $\psi(\mathbf{x})$ is the mother wavelet, $\det(\mathbf{A})$ is the determinant of the matrix $\mathbf{A}$, and $\mathbf{A}$ and $\mathbf{C}$ are anisotropy and linear transformation matrices, respectively, given by

$$\mathbf{A} = \frac{1}{a}\begin{bmatrix} L & 0 \\ 0 & 1 \end{bmatrix}, \tag{7}$$

and

$$\mathbf{C} = \begin{bmatrix} \cos\theta & \sin\theta \\ -\sin\theta & \cos\theta \end{bmatrix}. \tag{8}$$

A wavelet is a function that has unit energy ($\int |\psi(\mathbf{x})|^2 d\mathbf{x} = 1$), a zero mean, and is non-zero over a finite region (Farge, 1992). In this work we use the Morlet wavelet, defined as (e.g. Farge, 1992)

$$\psi(\mathbf{x}) = \frac{1}{\sqrt{\pi}} e^{i\mathbf{k_o}\cdot\mathbf{x}} e^{-\frac{1}{2}(\mathbf{x}\cdot\mathbf{x})}, \tag{9}$$

where $\mathbf{k_o} = [0, k_o]$, and $k_o > 5.5$. We use $k_o = 2\pi$. Figure 1 shows the real part of the Morlet wavelet with the effects of changing the scale (a), orientation (θ), and anisotropy ratio (L). Because the wavelet is non-zero only over a finite region, the wavelet transform identifies local properties of the field. The integral transform in (5) is evaluated for a range of shift parameters, $\mathbf{b}$, a range of scale parameters, a, and a range of orientations, θ. Shifting the wavelet in (5) results in the wavelet analysis of different regions of the field; scaling the wavelet analyzes varying sizes of regions within the field, and rotating the wavelet analyzes different orientations of the field. In our analysis, we hold L

constant.

Continuous wavelet analysis transforms a two-dimensional field, $f(\mathbf{x})$, into a four-dimensional $(a, \mathbf{b}, \theta)$ wavelet coefficient. To reduce the dimensionality, the four-dimensional wavelet coefficient is integrated over the $\mathbf{b}$ domain to obtain the wavelet variance, $WV_f(a, \theta)$, given by (Antoine et al., 2004)

$$WV_f(a, \theta) = \int_\Omega |W^\theta(a, \mathbf{b}, \theta; L)|^2 d\mathbf{b}, \tag{10}$$

where Ω is the domain of $\mathbf{b}$. Because integration is carried out over the $\mathbf{b}$ (spatial) domain, all local information is lost; thus the wavelet variance is a global measure. Large values of the wavelet variance occur at (a, θ) pairs that correspond to scales and orientations that exist anywhere in the field $f(\mathbf{x})$. Let us define these dominant scales and orientations as $a_{\max}$ and $\theta_{\max}$, respectively. These are globally-dominant scales and orientations. The locally-dominant orientation at each position $\mathbf{b} \in \mathbf{x}$ is the orientation, θ, at which the wavelet coefficient achieves its maximum value for a scale of $a_{\max}$, and is given by

$$\theta_{\max}(\mathbf{b}) = \{\theta : W^\theta(a_{\max}, \mathbf{b}, \theta; L) = \max(W^\theta(a_{\max}, \mathbf{b}, \theta; L))\}. \tag{11}$$

Procedure

Neupauer et al. (2006) used wavelet analysis to identify dominant orientations of permeability anisotropy according to the following procedure:

(1) Use (5) to calculate the wavelet coefficients for a range of shifts ($\mathbf{b} \in \mathbf{x}$), scales, and orientations, and for a particular anisotropy ratio, L.

(2) Use these wavelet coefficients in (10) to compute the wavelet variance.

(3) Determine the globally-dominant scales and orientations $(a_{\max}, \theta_{\max})$ by identifying the (a, θ) pairs that correspond to local maxima of the wavelet variance.

(4) Identify the locally-dominant orientations for each globally dominant scale, $a_{\max}$, using (11).

If a field contains two or more globally-dominant scales and orientations $(a_{\max}, \theta_{\max})$, the wavelet variance should have local maxima at each globally-dominant pair. However, if the $(a_{\max}, \theta_{\max})$ pair is not sufficiently distinct, the wavelet variance may only have one local maximum at an $(a_{\max}, \theta_{\max})$ that corresponds to the scale and orientation of the primary feature (Neupauer et al., 2006). To address this situation, we have developed a continuation of the procedure to identify $(a_{\max}, \theta_{\max})$ for a secondary feature. The procedure continues as follows:

(5) If the wavelet variance has only one local maximum, filter out the wavelet coefficients that correspond to $(a_{\max}, \theta_{\max})$ to remove the primary feature from the original field.

(6) Reconstruct the field with the remaining wavelet coefficients. For anisotropic wavelet analysis, the field $f(\mathbf{x})$ can be reconstructed from its wavelet coefficients using (adapted from Chui, 1992; Farge, 1992)

$$f(\mathbf{x}) = \frac{2}{\sqrt{L} C_\delta} \int_0^\pi \int_0^\infty \frac{W^\theta(a, \mathbf{b}, \theta; L)}{a^2} da d\theta, \tag{12}$$

where

$$C_\delta = \iint \frac{\hat{\psi}(u, v)}{u^2 + v^2} du dv, \tag{13}$$

where $\hat{\psi}(u, v)$ is the Fourier transform of the wavelet, and u and v are transform variables.

(7) Repeat Steps 1–4 for the reconstructed field to identify the secondary dominant orientation.

Implementation

To perform wavelet analysis, the integral transform in (5) is analyzed for a range of scales, shifts, and orientations. To reduce the computational burden, the integral transform can be evaluated in Fourier space, which eliminates the need to integrate over the range of shifts, $\mathbf{b}$. Substituting (6) into (5) gives

$$W^{\theta}(a, \mathbf{b}, \theta; L) = \sqrt{\det(\mathbf{A})} \int f(\mathbf{x})\psi^{*}(\mathbf{AC}(\mathbf{x} - \mathbf{b}))d\mathbf{x}. \tag{14}$$

The integral in this equation can be written as a convolution, leading to

$$W^{\theta}(a, \mathbf{b}, \theta; L) = \sqrt{\det(\mathbf{A})} f(\mathbf{b}) * \psi^{*}(-\mathbf{ACb}), \tag{15}$$

where $*$ denotes convolution. The convolution can be evaluated efficiently in Fourier space as a product of the Fourier transforms of $f(\mathbf{b})$ and $\psi^{*}(-\mathbf{ACb})$; thus the wavelet transform becomes

$$W^{\theta}(a, \mathbf{b}, \theta; L) = \sqrt{\det(\mathbf{A})} \mathcal{F}^{-1} \left\{ \mathcal{F}[f(\mathbf{b})]\mathcal{F}[\psi^{*}(-\mathbf{ACb})] \right\}, \tag{16}$$

where $\mathcal{F}$ and $\mathcal{F}^{-1}$ denote the Fourier and inverse Fourier transforms, respectively. This equation is evaluated for a range of scales and orientations.

EXAMPLE

In this section we demonstrate the wavelet analysis procedure using two-dimensional sinusoidal fields defined as

$$z_i(x, y) = \sin\left[\frac{2\pi}{T_i}(x\cos\phi_i + y\sin\phi_i)\right] \tag{17}$$

where ϕ_i is the orientation angle (defined as positive in the counterclockwise direction, with $\phi_i = 0$ in the direction of $+x$), T_i is the period, i denotes the case number, and the domain is -5 m$< x < 5$ m and -5 m$< y < 5$ m. We consider two cases. In Case 1 (Fig. 2A), the field contains two zones with sufficiently distinct scales and orientations, given by

$$(\phi_1, T_1) = \begin{cases} (45°, 1 \text{ m}), & x \leq 1 \text{ m} \\ (135°, 2 \text{ m}) & x > 1 \text{ m} \end{cases}. \tag{18}$$

We use this case to verify the procedure for identifying locally-dominant scales. In Case 2 (Fig. 3A), the field contains two zones with similar scales and orientations, given by

$$(\phi_2, T_2) = \begin{cases} (30°, 2 \text{ m}), & x \leq 1 \text{ m} \\ (20°, 1.6 \text{ m}) & x > 1 \text{ m} \end{cases}. \tag{19}$$

We use this case to demonstrate the filtering procedure.

Case 1: Two Zones with Distinct Periods and Orientations

We use wavelet analysis to identify the scale and orientation pairs that are dominant throughout the field $z_1(x, y)$ (Fig. 2A). We evaluate (16) for a range of scales ($a = 0.2, 0.3, \ldots, 4$ m) and orientations ($\theta = 0°, 5°, \ldots, 175°$), and we calculate the wavelet variance using (10). The results (Fig. 2B) show two local maxima in the wavelet variance – one at $(a_{\max}, \theta_{\max}) = (1 \text{ m}, 45°)$, and one at $(a_{\max}, \theta_{\max}) = (2 \text{ m}, 135°)$. These (a, θ) pairs represent the globally-dominant scales and orientations of the field and are identical to the true scales and orientations in (18). Note that since we use $k_o = 2\pi$ in (6), the local maxima of the wavelet variance occurs at a wavelet scale $a_{\max}$ that is equal to the period, T, of the sinusoidal function (Torrence and Compo, 1998; Neupauer et al., 2006). For $k_o \neq 2\pi$, $a_{\max}$ is a function of T, but is not identically equal to T.

The local maxima of the wavelet variance identify globally-dominant scales and orientations, but they do not provide information about the locally-dominant orientations. To identify the orientation that is dominant at each location, we use (11) for each of the dominant scales identified above. Figure 2C shows the dominant orientations at each position for $a = 2$ m. This wavelet scale is equal to the true period ($T = 2$ m) of the field for $x > 1$ m. The dominant orientation for $x > 1$ m is identified as 135°, which matches the true orientation of the field in this region. For $a = 1$ m, the dominant orientations at each location are shown in Figure 2D. This wavelet scale is equal to the true period ($T = 1$ m) of the field for $x < 1$ m. For $x < 1$ m, the dominant orientation of the field is identified as 45°, which matches the true orientation of the field in this region. The present method does not identify the location of the interface between the two zones with different orientations. This is the subject of future work.

Case 2: Two Zones with Similar Periods and Orientations

We use wavelet analysis to identify the scale and orientation pairs that are dominant throughout the field $z_2(x, y)$ (Fig. 3A). We evaluate (16) for a range of scales ($a = 0.2, 0.3, \ldots, 4$ m) and orientations ($\theta = 0°, 2°, \ldots, 178°$), and we calculate the wavelet variance using (10). The results (Fig. 3B) show one local maximum at $(a_{\max}, \theta_{\max}) = (2 \text{ m}, 30°)$, which represents the scale and orientation of the more dominant (primary) zone of the field, i.e., $x < 1$ m. This zone is more dominant because it covers a larger area of the domain, and because it has a larger period. Although the field contains two zones with different periods and orientations, the periods and orientations are sufficiently similar so that the regions with large wavelet variance values overlap, and the region containing the primary (a,θ) pair masks the region containing the secondary (a,θ) pair.

We filter $z_2(x, y)$ to remove the part that has a dominant orientation of 30°. We accomplish this by reconstructing $z_2(x, y)$ from (12) using only a subset of the wavelet coefficients. To choose the subset of wavelet coefficients to use in the reconstruction, we select a threshold value of the wavelet variance so that the field is reconstructed using only the wavelet coefficients that correspond to wavelet variance values that are above the threshold. We use a threshold value of 61.5 m^4, which was chosen such that 75% of the total wavelet variance is above the threshold. Figure 4A shows the wavelet variance of $z_2(x, y)$ with only values below the threshold wavelet variance remaining.

Using (12), we reconstruct $z_2(x, y)$ using only the remaining wavelet coefficients (Fig. 4B). Let us denote this filtered version by $\overline{z}_2(x, y)$. Note that

$\overline{z}_2(x, y)$ approximates $z_2(x, y)$ for $x > 1$ m (the less dominant zone); while for $x < 1$ m (the more dominant zone), $\overline{z}_2(x, y) \approx 0$. Thus, the primary feature of the original field has been removed. Note that the reconstruction is not exact near the boundaries of the domain or at the boundaries between the two zones.

Finally, we perform wavelet analysis on $\overline{z}_2(x, y)$ to obtain its wavelet variance. The wavelet variance (Fig. 4C) has a local maximum at $(a_{\max}, \theta_{\max}) = (1.6$ $\mathrm{m}, 14°)$. This $a_{\max}$ is identical to the period of $z_2(x, y)$ for $x > 1$ m, and this $\theta_{\max}$ is approximately equal to the orientation of $z_2(x, y)$ for $x > 1$ m. Thus, the combination of filtering, reconstruction, and reanalysis allows us to identify the secondary feature of $z_2(x, y)$.

To identify the orientation that is dominant at each location, we use (11) for the two dominant scales identified above. Figure 3C shows the locally-dominant orientations for $a = 2$ m, which is the true period for $x < 1$ m. The wavelet analysis procedure correctly identifies the locally-dominant orientation to be 30° in this zone ($x < 1$ m). Figure 3D shows the dominant orientations at each position for $a = 1.6$ m, which is the true period for $x > 1$ m. The wavelet analysis procedure correctly identifies the locally-dominant orientation to be 20° in most of this zone; however, the identified dominant orientation is slightly off near the interface between the two zones.

APPLICATION TO MASSILLON SANDSTONE DATA

Tidwell and Wilson (2000) collected permeability measurements (Fig. 5A) on a $0.94 \times 0.96 \times 1.01$ m block of Massillon sandstone using a gas multisupport permeameter. These measurements were taken on a square 50-by-50 grid at a spacing of $dx = dy$ =0.0127 m. The 0.622×0.622 m grid was centered on the block face providing a buffer of over 0.15 m between the grid and edge of the block to avoid boundary effects. The Massillon sandstone exhibits a series of subhorizontal bounding surfaces with low permeability (spacing of 0.16-0.22 m; orientation of $\theta \approx 0°$; Tidwell and Wilson, 2000) separated by cross-stratification sets with high permeability (spacing of approximately 0.03 m; orientation of $\theta \approx -22°$; Tidwell and Wilson, 2000).

Neupauer et al. (2006) performed wavelet analysis on the Massillon permeability data, but the wavelet analysis results only identified the bounding surfaces, which is a more dominant feature than the cross stratification sets. In this section, we use the combined wavelet analysis and filtering technique to characterize the dominant orientation of both the bounding surfaces and the cross stratification sets.

We performed wavelet analysis on the Massillon permeability data and calculated the wavelet variance using (10). We used a range of scales of $a = 3dx, 4dx, \ldots, 0.3937$ m, and an anisotropy ratio of $L = 0.2$. (Powell (2004) found that $L = 0.2$ gave the best representation of the dominant orientations for these data.) The wavelet variance (Fig. 5B) has one local maximum at $(a_{\max}, \theta_{\max}) = (0.1819\text{ m}, 0°)$, which corresponds to the separation distance and orientation of the bounding surfaces. We would also expect a local maximum at $(a_{\max}, \theta_{\max}) \approx (0.03\,\text{m}, -22°)$, corresponding to the cross-stratification sets; however, this maximum is masked by the high wavelet variance values corresponding to the bounding surfaces. We implement the filtering method to remove the primary feature (bounding surfaces) from the field so that the secondary feature (cross-stratification sets) can be identified.

We filter the Massillon permeability data by reconstructing the data with the wavelet coefficients corresponding to the wavelet variance values below the threshold value (4.9×10^{-29} m^8, the value that removes 75% of the wavelet variance). The wavelet variance (Fig. 6A) from the remaining wavelet coefficients shows that the original local maxima is removed. The reconstruction of the permeability data from these remaining wavelet coefficients (Fig. 6B) shows that the low-permeability bounding surfaces are removed or subdued.

We perform wavelet analysis on the filtered data set to identify previously-masked secondary features. The resulting wavelet variance is shown in Figure 6C. The wavelet variance has a local maximum at $(a_{\mathrm{max}}, \theta_{\mathrm{max}}) = (0.0508\,\mathrm{m}, -20^\circ)$. This orientation closely matches the orientation (-22°) that Tidwell and Wilson (2000) identified in their variogram analysis. Through visual inspection of the Massillon permeability data, Tidwell and Wilson (2000) identified the separation distance of cross-stratification sets to be slightly less (approximately 0.03 m) than the results of our wavelet analysis.

For the secondary dominant scale ($a = 0.0508$ m), we use (11) to identify the locally-dominant orientations (Fig. 6D). Throughout most of the domain, the dominant orientations range from -30° to 0°, which matches the dominant orientation of the cross-stratification sets. Near $y \approx 0.7$ m the identified locally-dominant orientation is $\theta \approx 0^\circ$. This is consistent with the reconstructed data (Fig. 6B) in that region, and indicates that the filtering subdued, but did not completely remove, the bounding surface in that region. Similar behavior is seen near $y \approx 0.55$ m for $x < 0.6$ m. In the lower right corner of the domain, the identified locally-dominant orientations are nearly vertical, which matches both the original data (Fig. 5A) and the filtered data (Fig. 6B). Since filtering only removed wavelet coefficients that correspond to $\theta \approx 0^\circ$, in this region where the dominant orientation is $\theta \approx 90°$, the filtered data have the same dominant orientation as the original data.

CONCLUSION

In this paper, we presented a wavelet analysis approach that can be used to identify dominant orientations in both stationary and non-stationary permeability fields. We addressed a class of non-stationarity in which the permeability field contains zones with different dominant orientations and scales, but within a given zone, the properties are stationary.

Wavelet analysis involves the integral transform of a data set using a wavelet as a kernel. The result of the integral transform is a set of wavelet coefficients that are used to obtain the wavelet variance. Large values of the wavelet variance occur at globally-dominant scales and orientations. If a permeability field contains two zones with distinct dominant scales and orientations, the wavelet variance will have two distinct local maxima, and the dominant scales and orientations can easily be identified. If the permeability field contains two zones with similar dominant scales and orientations, the wavelet variance may only have one local maximum, with the wavelet variance of the primary region masking the wavelet variance of the secondary region. In this paper, we developed a filtering approach that is used in conjunction with wavelet analysis to identify both primary and secondary features.

In the filtering approach, the original data are filtered by removing all wavelet coefficients that correspond to wavelet variance values above a chosen threshold. The filtered data are reconstructed from only the remaining wavelet coefficients, thus eliminated or subduing the more dominant features of the original data. We have obtained reasonable results by using a threshold value such that 75% of the wavelet variance is removed. We illustrated the new filtering method using laboratory-collected permeability data from Massillon sandstone. The Massillon sandstone is characterized by low-permeability subhorizontal bounding surfaces that separate low angle cross-stratification sets (Tidwell and Wilson, 2000). In prior work (Neupauer et al., 2006), wavelet analysis was used to identify dominant orientations in the Massillon sandstone permeability data; however, it was able to identify only the primary feature (bounding surfaces). With the new combined wavelet analysis and filtering approach, we identified both the primary (bounding surfaces) and secondary (cross-stratification sets) features.

References

[1] Anderman, E.R., Kipp, K.L., Hill, M.C., Valstar, and Neupauer, R.M., 2002, MODFLOW-2000, The U.S. Geological Survey Modular Ground-Water Model – Documentation of the Model-Layer Variable-Direction Horizontal Anisotropy (LVDA) Capability of the Hydrogeologic-Unit Flow (HUF) Package, U.S. Geological Survey, Open file Report 02-409.

[2] Antoine, J., Murenzi, R., Vandergheynst, P., and S.T. Ali, 2004, Two-Dimensional Wavelet and their Relatives: Cambridge University Press, Cambridge, 458 pp.

[3] Bear, J., 1972, Dynamics of Fluids in Porous Media: American Elsevier, New York, 764 pp.

[4] Beckwith, C.W., Baird, A.J., and Heathwaite, A.L., 2003, Anisotropy and depth-

related heterogeneity of hydraulic conductivity in a bog peat. II: Modelling the effects on groundwater flow: Hydrol Process, v. 17, p. 103–113.

[5] Burton, W.C., Plummer, L.N., Busenberg, E., Lindsey, B.D., and Gburek, W.J., 2002, Influence of Fracture Anisotropy on Groundwater ages and chemistry, Valley and Ridge Province, Pennsylvania, Ground Water, vol. 40, no. 3, p. 242–257.

[6] Chen, X.H., and Chen, X., 2003, Effects of Aquifer Anisotropy on the Migration of Infiltrated stream water to a pumping well: Jour. Hydrologic Engr. ASCE, vol. 8, no. 5, p. 287–293.

[7] Chui, C.K., 1992, An Introduction to Wavelets: Academic Press, California, 113 pp.

[8] Farge, M., 1992, Wavelet Transforms and Their Applications to Turbulence: Annu. Rev. Fluid Mech., v. 24. 395–457.

[9] Genereux, D., and Bandopadhyay, I., 2001, Numerical investigation of lake bed seepage patterns: Effects of porous medium and lake properties: Jour. Hydrology, vol. 241, no. 3-4, p. 283–303.

[10] Isaaks, E.H., and Srivastava, R.M., 1989, An Introduction to Applied Geostatistics: Oxford University Press, New York, 561 pp.

[11] Neupauer, R.M., Powell, K.L., Qi, X., Lee, D.H. and Villhauer, D.A., 2006, Characterization of permeability anisotropy using wavelet analysis: Water Resour. Res., v. 42, *doi:, pages.*

[12] Powell, K.L., 2004, Wavelet Analysis of Permeability Anisotropy: Master's Thesis, University of Virginia, 89 pp.

[13] Tidwell, V.C., and Wilson, J.L., 2000, Heterogeneity, Permeability patterns, and Permeability upscaling: Physical Characterization of a block of Massillon

Sandstone exhibiting Nested Scales of Heterogeneity: SPE Reserv. Eval. Eng., v. 3, no. 4, p. 283–291.

[14] Torrence, C., and Compo, G.P., 1998, A Practical guide to Wavelet Analysis: Bull. Amer. Meteor. Soc. , vol. 79, no. 1, p. 61–78.

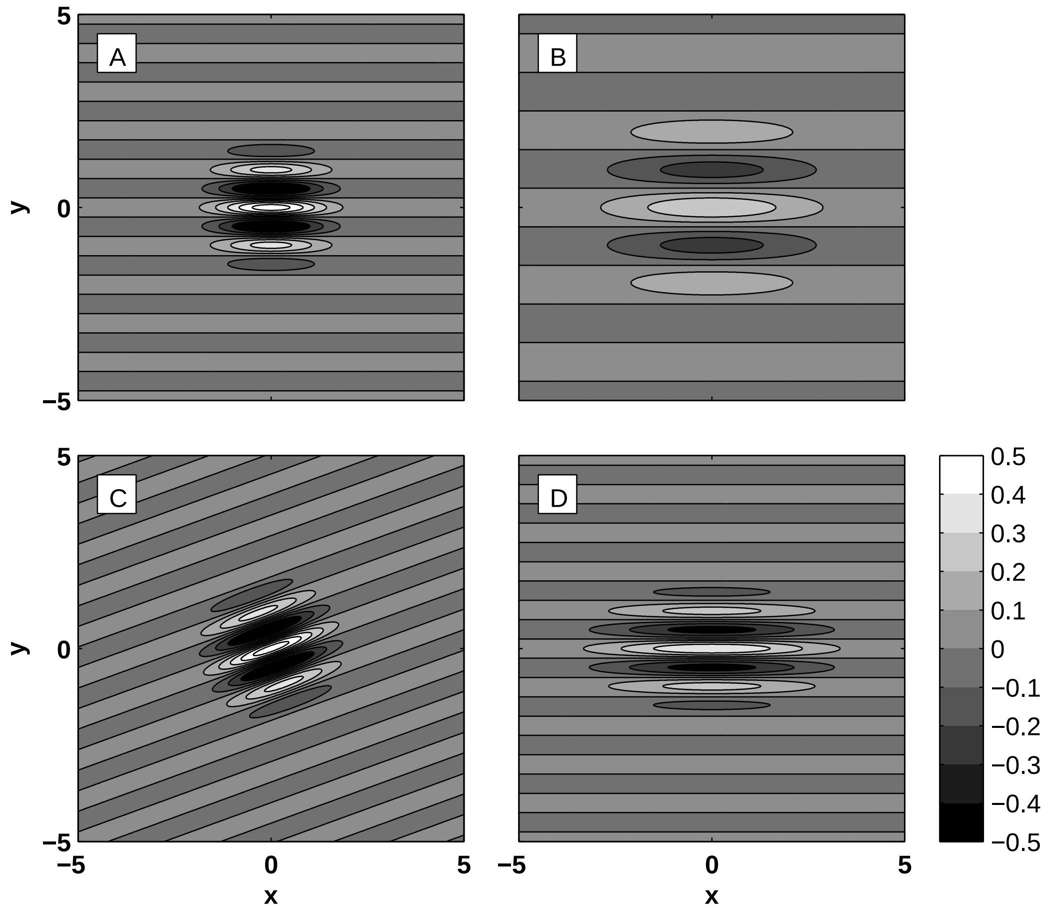

Fig. 1. Morlet wavelet (real part only). (A) $a = 1, \mathbf{b} = (0, 0)$, $\theta = 0°$, $L = 1$; (B) $a = 2, \mathbf{b} = (0, 0)$, $\theta = 0°$, $L = 1$; (C) $a = 1, \mathbf{b} = (0, 0)$, $\theta = 20°$, $L = 1$; (D) $a = 1, \mathbf{b} = (0, 0)$, $\theta = 0°$, $L = 1/2$.

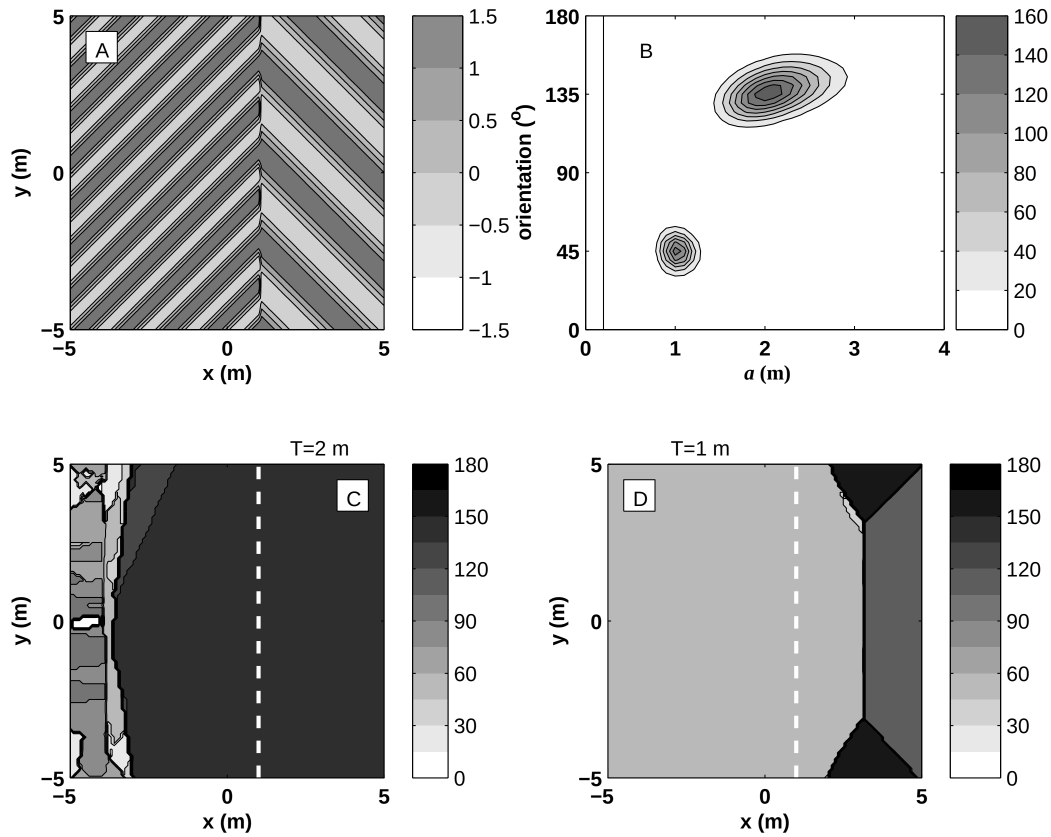

Fig. 2. Wavelet analysis of $z_1(x, y)$. (A) $z_1(x, y)$; (B) Wavelet variance (m^4); (C) Locally-dominant orientations (in degrees) for $a = 2$ m; (D) Locally-dominant orientations (in degrees) for $a = 1$ m. The dashed white line denotes the interface between the two zones. The labels above subplots C and D show the true period of the field, in the region where the true period matches the scale of the analyzing wavelet.

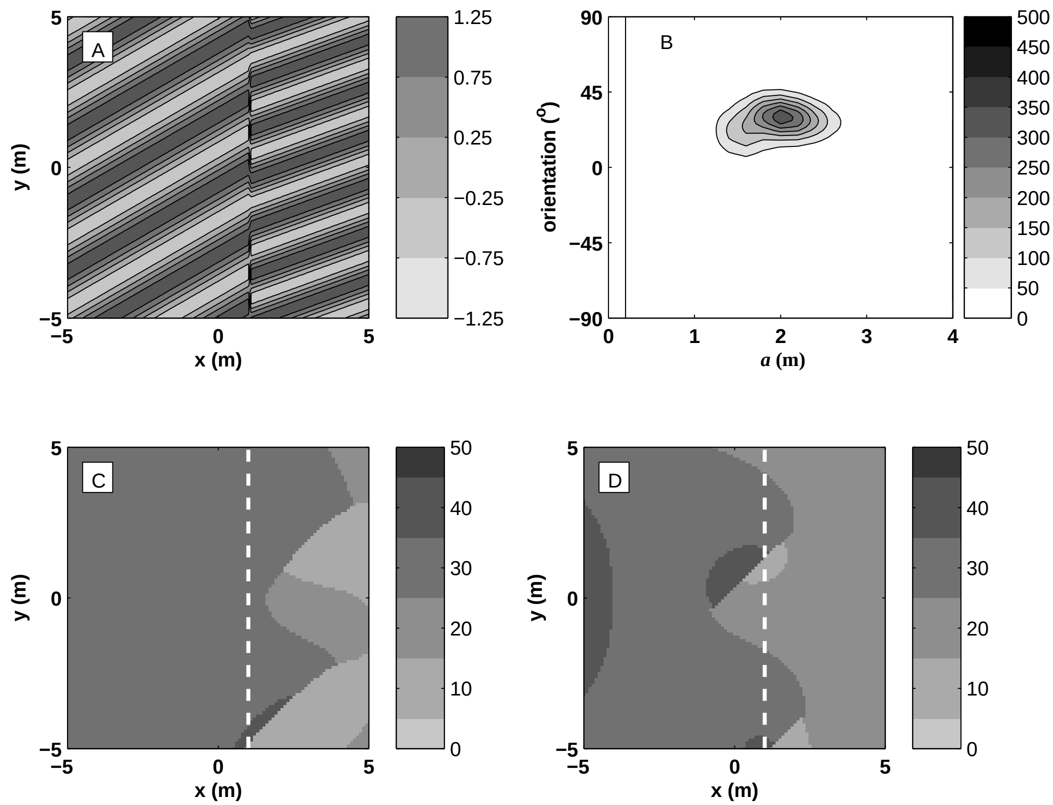

Fig. 3. Wavelet analysis of $z_2(x, y)$. (A) $z_2(x, y)$; (B) Wavelet variance (m^4); (C) Locally-dominant orientations (in degrees) for $a = 2$ m; (D) Locally-dominant orientations (in degrees) for $a = 1.6$ m. The dashed white line denotes the interface between the two zones.

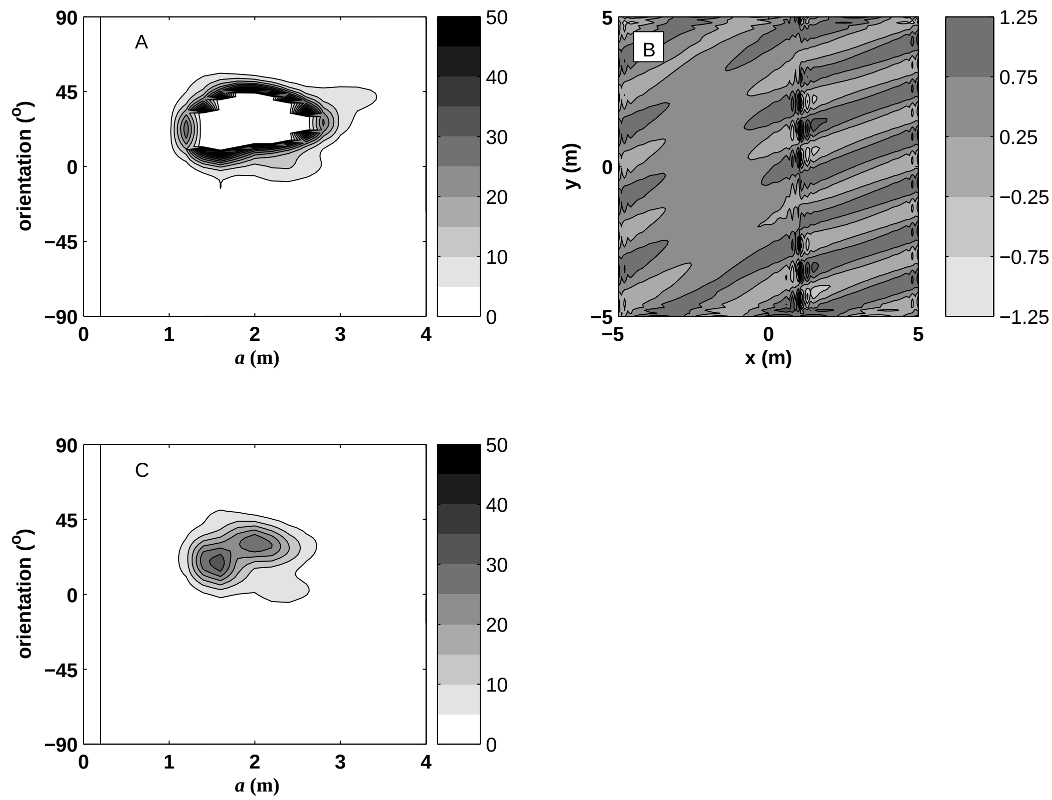

Fig. 4. Filtering and re-analysis of $z_2(x,y)$. (A) Wavelet variance with only values below the threshold value of 61.5 m^4 (m^3); (B) $\overline{z}_2(x,y)$; (C) Wavelet variance of $\overline{z}_2(x,y)$ (m^3).

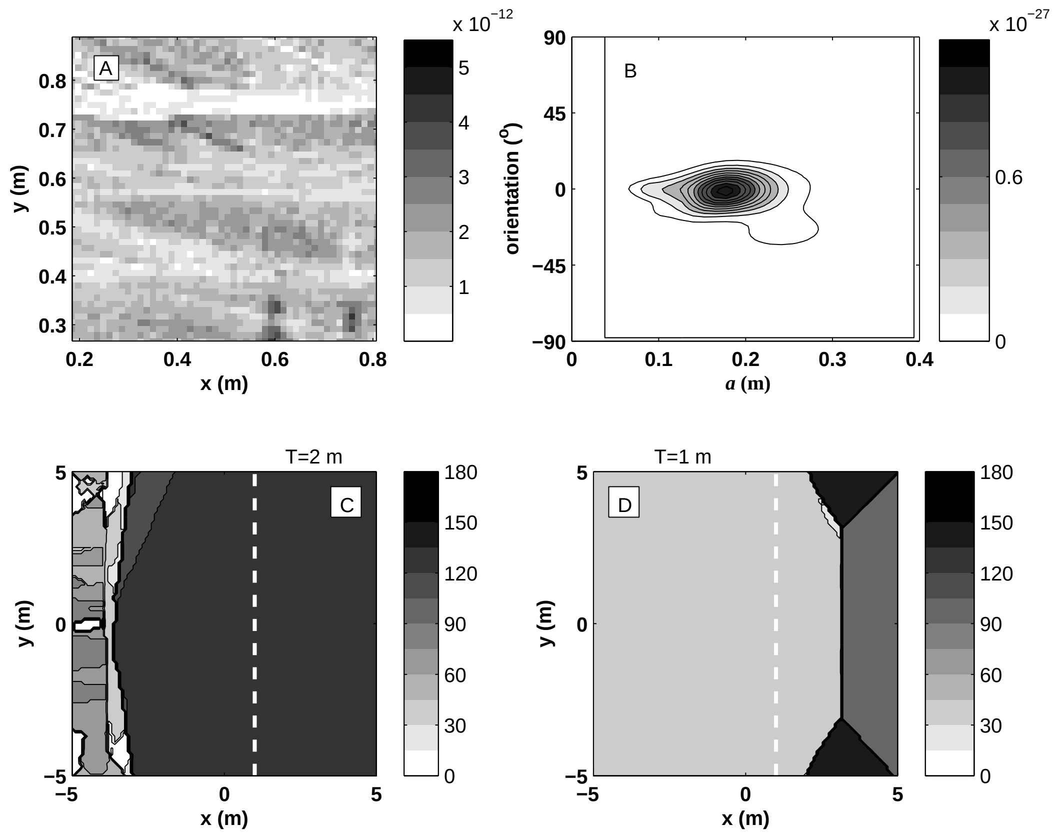

Fig. 5. Analysis of Massillon permeability data. (A) Permeability measurements (m^2). (B) Wavelet variance. (m^8).

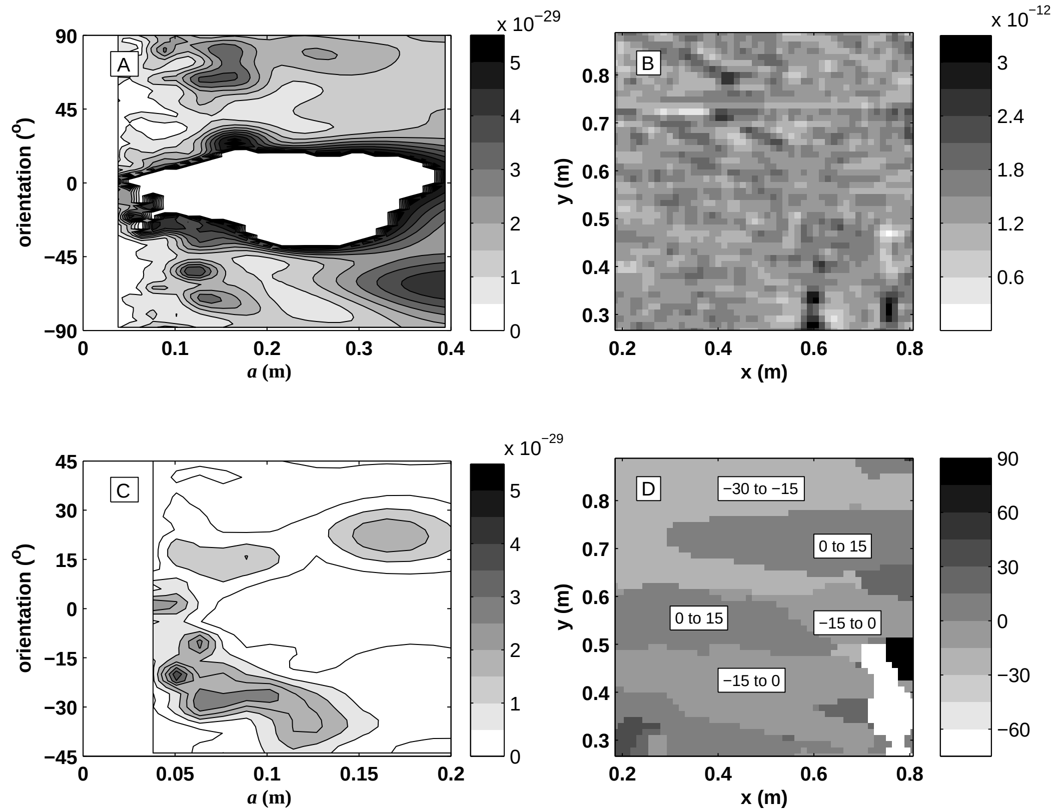

Fig. 6. Filtering, reconstruction and reanalysis of Massillon permeability data. (A) Filtered wavelet variance. (m^8). (B) Reconstruction of the Massillon permeability data from the filtered wavelet coefficients (m^2). (C) Wavelet variance of reconstructed Massillon permeability data (m^8). (D) Dominant orientations at each location at a wavelet scale of $a = 0.0508$ m.